

# Microwave state transfer and adiabatic dynamics of magnetically trapped polar molecules

Benjamin K. Stuhl,\* Mark Yeo, Brian C. Sawyer,† Matt Hummon, and Jun Ye  
*JILA, National Institute of Standards and Technology and University of Colorado,  
 Department of Physics, 440 UCB, Boulder, Colorado 80309, USA*

Cold and ultracold polar molecules with nonzero electronic angular momentum are of great interest for studies in quantum chemistry and control, investigations of novel quantum systems, and precision measurement. However, in mixed electric and magnetic fields, these molecules are generically subject to a large set of avoided crossings among their Zeeman sublevels; in magnetic traps, these crossings lead to distorted potentials and trap loss from electric bias fields. We have characterized these crossings in OH by microwave-transferring trapped OH molecules from the upper  $|f; M = +\frac{3}{2}\rangle$  parity state to the lower  $|e; +\frac{3}{2}\rangle$  state and observing their trap dynamics under an applied electric bias field. Our observations are very well described by a simple Landau-Zener model, yielding insight to the rich spectra and dynamics of polar radicals in mixed external fields.

PACS numbers: 37.10.Pq, 33.80.Be, 33.20.-t

Cold polar molecule experiments have made a remarkable transformation over the past decade, progressing all the way from the first demonstrations of basic motional control of molecules [1–3] to studies in ultracold chemistry [4], polar collisions [5–7], and precision measurement [8, 9]. Closed-shell molecules at low temperatures and long ranges present nearly featureless electric dipoles [10, 11], yielding universal scattering behavior and the prediction of generic dipolar condensates [12] or crystals [13]. At shorter ranges, the quantum statistics and chemical nature of the specific species comes to the forefront [4, 14]. Polar *radicals* behave in even richer fashions: topological crystals [15], half-integer vortices generated by conical intersections [16], and spin-dependent chemistry [17] have been predicted, and the utility of using magnetic fields to trap radicals while performing electric-dipole-dependent studies has already been demonstrated [14, 18, 19]. Motivated by these predictions, several groups are pursuing the production of ultracold radicals such as RbSr [19, 20] and LiYb [21].

While the combination of electric and magnetic dipoles enables fascinating new phenomena, it also comes with substantial complications. In particular, simple linear Zeeman spectra are converted to tangles of interwoven avoided crossings by the application of remarkably small transverse electric fields. In this Letter, we report the experimental observation of these crossings in the polar radical OH and their dramatic impact on dynamics in a magnetic trap. In its  ${}^2\Pi_{3/2}$  ground electronic state, stationary OH has a magnetic dipole moment of  $2\mu_B$  (where  $\mu_B$  is the Bohr magneton) and an electric moment of 1.67 D (0.65 a. u.); rotational averaging reduces each of these in the laboratory frame to  $\mu_i^{(eff)} = \mu_i \frac{M\bar{\Omega}}{J(J+1)}$ , where  $J$  is the total angular momentum,  $M$  is its lab-fixed projection, and  $\bar{\Omega}$  is the magnitude of  $J$ 's projection on the internuclear axis. Each rotational level of OH contains two Zeeman manifolds of opposite parity,

$|e; M\rangle$  and  $|f; M\rangle$ ; with no applied fields, these states are split by a  $\Lambda$ -doublet coupling of 1.667 GHz. In an applied electric field,  $|e\rangle$  and  $|f\rangle$  are not strictly good quantum numbers. However, they are still useful as labels of a state's Stark character:  $|e\rangle$  states are strong-electric-field-seeking while  $|f\rangle$  states are weak-field-seeking.

A representative Hamiltonian for  $\Lambda$ -doublet molecules in mixed electric and magnetic fields has been derived in [22]. While realistic systems must be solved numerically, the basic structure of the combined  $H_{total} = H_{zero-field} + H_{Stark} + H_{Zeeman}$  Hamiltonian is simple: the zero-field part generates diagonal matrix elements in a suitable basis (e. g. Hund's case A fine-structure plus parity basis  $|JM\bar{\Omega}\epsilon\rangle$  for OH, where  $\epsilon = e$  or  $f$  is the  $J$ -relative parity label), as does the Zeeman part if one takes the space-fixed  $Z$  axis to lie along the magnetic field  $\vec{B}$ . The off-diagonal elements are then purely from the Stark portion. The component of the electric field  $\vec{E}$  parallel to  $\vec{B}$  generates matrix elements which preserve  $M$  and change the parity  $\epsilon$ , while the transverse components change  $M$  by  $\pm 1$  as well as  $\epsilon$ . As can be seen in the Zeeman spectrum of OH (Fig. 1(a)), all states in the lower parity manifold except for the absolute ground state have Zeeman-induced crossings with one or more of the upper parity states: in an E-field, these real crossings are coupled by the off-diagonal Stark elements and become avoided. Working in the perturbative limit, the crossings  $X_M$  of Fig. 1 have widths  $\delta_{+1/2} \propto |E \sin \theta_{EB}|$ ,  $\delta_{-1/2} \propto |E^3 \sin^2 \theta_{EB} \cos \theta_{EB}|$ , and  $\delta_{-3/2} \propto |E^3 \sin^3 \theta_{EB}|$ , where  $\theta_{EB}$  is the angle between  $\vec{E}$  and  $\vec{B}$ . Since the off-diagonal elements only couple states of opposite parity, the total perturbation theory order must be odd: crossings with total  $\Delta M$  even such as  $X_{-1/2}$  require one extra  $\Delta M = 0$  coupling order so that the total coupling changes  $\epsilon$  as it must. This mix of  $\Delta M = \pm 1$  and  $\Delta M = 0$  matrix elements in turn leads to a  $(\sin \theta_{EB})^{\Delta M} \cos \theta_{EB}$  angular dependence in the cou-

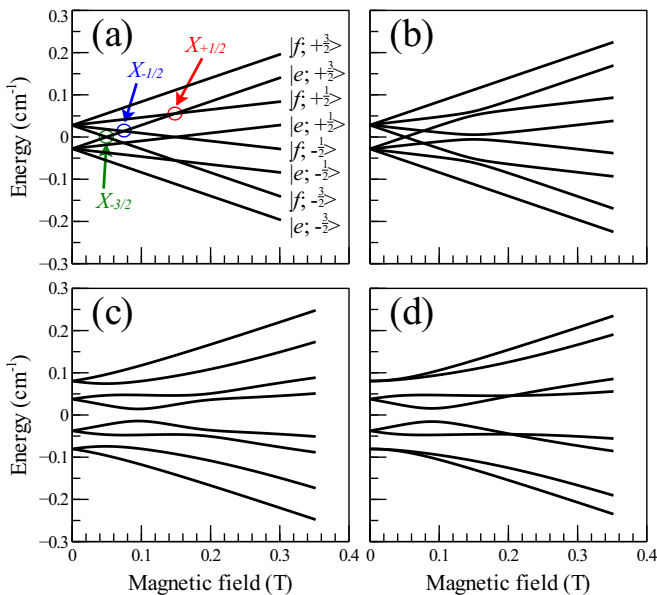


Figure 1. (color online) The Zeeman structure of OH with bias electric fields: (a) 0 V/cm, (b) 500 V/cm at a  $90^\circ$  magnetic-to-electric field angle  $\theta_{EB}$ , (c) 5000 V/cm at  $65^\circ$ , and (d) 5000 V/cm at  $90^\circ$ . The crossings  $X_M$  of the  $|e; +\frac{3}{2}\rangle$  state with the three  $|f; M = \{-\frac{3}{2}, -\frac{1}{2}, +\frac{1}{2}\}\rangle$  states are labeled in (a).

pling strengths for these even crossings, while the angular dependence for crossings with  $\Delta M$  odd is simply  $(\sin \theta_{EB})^{\Delta M}$ . Perturbation theory begins to fail, however, at relatively small  $E$ -fields (much smaller than the polarizing  $E$ -field at zero  $B$ -field) because of the strength of the electric dipole coupling and the fact that the Zeeman crossings are gapless at zero  $E$ -field. Therefore, for all calculations described in this Letter we diagonalize the full  $8 \times 8$  ground state fine-structure Hamiltonian of OH [23, 24].

We observe these avoided crossings by their dynamical effects on a sample of magnetically trapped OH molecules. Our Stark deceleration and magnetic trapping system has been described elsewhere [14]. Briefly, OH molecules are created in an electric discharge through water vapor in a supersonic expansion and then Stark decelerated and brought to rest in a permanent magnetic quadrupole trap (Fig. 2(a)) at a temperature of  $\sim 70$  mK, in their  $|f; +\frac{3}{2}\rangle$  state. By applying chirped microwave fields to the trap magnet surfaces, we can then transfer the trapped molecules to the  $|e; +\frac{3}{2}\rangle$  state, wherein we can probe the three crossings labeled in Fig. 1(a); application of a DC voltage to the magnets results in a bias  $E$ -field with the distribution shown in Fig. 2(b). The spatial loci of the three crossings in the actual field gradient of our trap are shown in Fig. 2(c). The multiple-well structure is a result of our use of permanent magnets: the hole in the center of the magnets allows flux to exit both inside and outside the magnet ring, yielding a toroidal field minimum between the faces of the magnet,

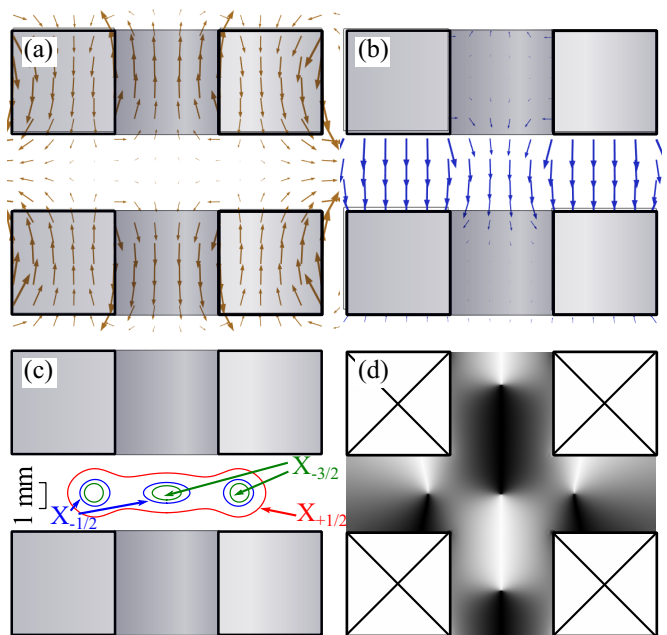


Figure 2. (color online, to scale) (a) The magnetic field distribution in the permanent magnet quadrupole trap. (b). The electric field distribution created by applying a potential difference to the trap magnets. (c) The spatial location of the avoided crossings  $X_M$ . (d) The relative angle  $\theta_{EB}$  between electric and magnetic fields in the trap. White denotes  $0^\circ$  while black denotes  $180^\circ$ , implying that the avoided crossings are widest in the gray regions.

as well as the central quadrupole trap. The distribution of  $\theta_{EB}$  angles generated by charging the magnets is plotted in Fig. 2(d).

As our trapped molecules are moving at velocities  $\lesssim 10$  m/s, only a very small energy gap is needed for each molecule to follow the adiabats rather than the diabats of the potential surfaces. As can be seen in Fig. 1, the adiabats of all the levels below the “doubly-stretched”  $|f; +\frac{3}{2}\rangle$  state are substantially less trapped than the  $|e; +\frac{3}{2}\rangle$  diabat – or in some cases, are outright antitrapped. Thus, if molecules are transferred to the  $|e; +\frac{3}{2}\rangle$  diabat in zero field and then a bias field is applied, some fraction of the molecules will leak out of the trap as they follow the adiabats rather than Landau-Zener hopping [25] to follow the trap diabat. At low fields, the Landau-Zener hopping probability is still substantial, and so it takes multiple trap oscillations for a molecule to leak out. At higher fields, however, effectively all molecules follow the adiabats and so the loss rate is simply limited by the trap dynamical time  $\tau_{dyn} = \frac{1}{4\nu_{trap}^{-1}}$  where  $\nu_{trap}$  is the trap oscillation frequency.

In order to transfer population from  $|f; +\frac{3}{2}\rangle$  to  $|e; +\frac{3}{2}\rangle$ , we use an Adiabatic Rapid Passage (ARP) technique [26] via microwave fields applied directly to the trap magnets. As the magnets also experience  $\pm 14$  kV

potentials as part of the trap loading sequence, the microwave system is AC-coupled to the trap by a pair of in-vacuum high voltage capacitors [23]. This capacitive coupling stage reduces the  $\pm 14$  kV bias to a few volts; two 1.2 GHz high-pass filters further suppress both the near-DC bias and the switching transients. By chirping our microwave frequency through the entire range of differential Zeeman shifts [8] in our trap over a period  $\tau_{ARP} \ll \tau_{dyn}$ , we are able to achieve transfer of  $\sim 75\%$  of the observable trap population. (Since the transfer is a  $\pi$  transition, only the fraction of  $\vec{E}_{RF} \parallel \vec{B}$  is useful. Thus, molecules in the gray regions of Fig. 2(d) see much smaller effective intensities than molecules in the white or black regions.)

In addition to causing dynamical trap loss, the avoided crossings  $X_M$  also reduce the efficiency of our ARP pulses: in the vicinity of the avoided crossings, not only are the states shifted away from the nominal 1.667 GHz transition frequency, but also the two parity states are mixed by the electric field. The net result of this mixing is that molecules transferred near said crossings may not in fact be transferred to the  $|e; +\frac{3}{2}\rangle$  diabat but rather may end up on the  $|f; M\rangle$  diabat and thus be invisible to our state-selective detection. Figure 3 displays the  $|e; +\frac{3}{2}\rangle$  population as a function of the DC bias field applied during the ARP. The bias field leads to a rapid drop in transferred population as the  $|f; +\frac{3}{2}\rangle \rightarrow |e; +\frac{3}{2}\rangle$  transition is Stark-shifted out of resonance; the bias field required for this shift increases with the frequency width of the ARP pulse. We have performed simulations using a numerical solution of the Optical Bloch Equations to calculate a position dependent ARP transfer probability with zero electric field. We then calculate the position-dependent Stark-Zeeman shift by diagonalizing the OH Hamiltonian and convolve the resulting frequency distribution with the ARP bandwidth to determine the total fraction transferred. The simulation results shown in Fig. 3 give a good match to the population measurements, showing that the ARP process is well-understood [23]. The simulations suggest the presence of a stray E-field in the trap region on the order of 100–150 V/cm.

Applied E-fields also have a profound effect on trap dynamics. A loss of  $\sim 40\%$  of the  $e$ -state population over  $\tau_{dyn}$  is observed immediately after the ARP pulse (Fig. 3 inset), almost certainly due to prompt loss of molecules following an adiabat through the  $X_{+1/2}$  crossing (which is fully avoided in just the observed stray E-field) and exiting the trap. At larger bias fields, loss rates up to  $2\tau_{dyn}^{-1}$  are observed with critical fields again on the order of 200–300 V/cm. The observed loss rates (Fig. 4(a)) are well-fit by a probabilistic model

$$\Gamma = \Gamma_{vacuum} + \tau_{dyn}^{-1} \times \sum_{M \in \{-\frac{3}{2}, -\frac{1}{2}\}} (1 - \mathcal{P}_{LZ}^{(M)})$$

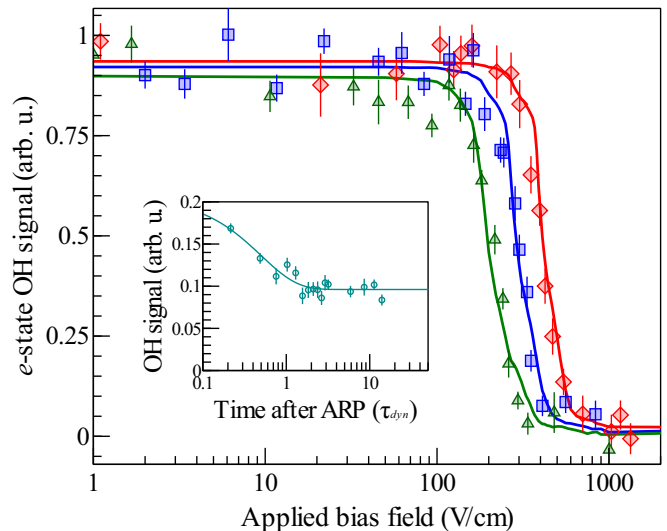


Figure 3. (color online) Post-ARP  $e$ -state population versus applied bias field, with 10 (green triangles), 20 (blue squares), and 40 MHz (red diamond) ARP chirp widths. Solid lines are Monte-Carlo simulations of the population transfer using realistic bias and RF field distributions from finite-element calculations, a semiclassical treatment of the Stark detunings, and a homogeneous stray field as a free parameter. (inset) Time-of-flight of  $e$ -state population immediately after ARP, with no applied bias field. The rapid loss through the  $X_{+1/2}$  crossing is clearly visible: the solid line is a fit to a single-exponential loss at a rate of  $2\tau_{dyn}^{-1}$ .

where  $\Gamma_{vacuum}$  is the background vacuum loss rate and

$$\mathcal{P}_{LZ}^{(M)} = \exp\left(-\frac{2\pi\xi \langle \delta_M^2(E_{eff}) \rangle}{\hbar (\Delta\mu_{eff}(M)) \langle \frac{dB}{dt} \rangle}\right)$$

is the Landau-Zener probability that the molecule stays on the  $|e; +\frac{3}{2}\rangle$  diabat through the crossing  $X_M$ . Angle brackets denote population averages:  $\langle \frac{dB}{dt} \rangle = \langle \vec{\nabla} B \cdot \vec{v} \rangle$  is the rate of change of the magnetic field and  $\langle \delta_M(E_{eff}) \rangle = \langle \delta_M(\sqrt{E^2 + E_{stray}^2}) \rangle$  is the width of the crossing  $X_M$  as a function of applied electric field  $E$  and stray field  $E_{stray}$ , while  $\Delta\mu_{eff}(M) = \left(\frac{3/2 \cdot 3/2}{3/2 \cdot 5/2} - \frac{3/2 \cdot M}{3/2 \cdot 5/2}\right) \cdot 2\mu_B$  is the difference between the effective magnetic moments of the  $|f; +\frac{3}{2}\rangle$  and  $|e; M\rangle$  states. The model contains only 3 free parameters:  $\Gamma_{vacuum}$ ,  $E_{stray}$ , and  $\xi \approx 0.12$ , which incorporates the errors in our estimates of the population-averaged parameters. (While we can estimate  $\langle \frac{dB}{dt} \rangle$  reasonably well from Monte-Carlo trap dynamics simulations,  $\langle \delta_M(E_{eff}) \rangle$  has a very fast variation with  $\langle \theta_{EB} \rangle$  and so is hard to accurately calculate. It is therefore responsible for most of  $\xi$ 's deviation from unity.)  $\Gamma_{vacuum}$  can be independently observed from the  $f$ -state lifetime, while  $E_{stray}$  can be derived from Fig. 3; both of these independent measurements are consistent with the fit.  $\tau_{dyn}$  is directly measurable from the trap os-

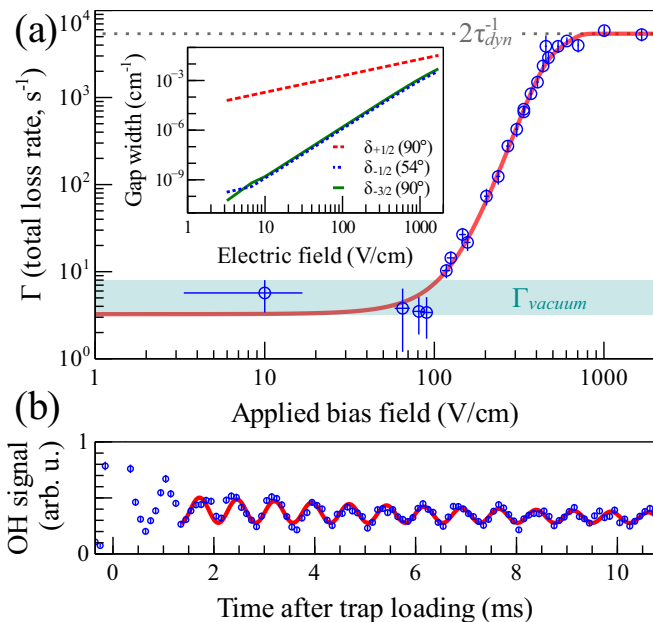


Figure 4. (color online) (a) Loss rate of  $|e; M = +\frac{3}{2}\rangle$  molecules versus applied electric field. The solid red line is a fit to a simple Landau-Zener model; the green shaded stripe denotes the range of observed loss rates for  $|f; +\frac{3}{2}\rangle$  molecules. The bias field is turned on 5 ms after the ARP pulse is completed, and thus well after the prompt loss seen in the inset of Fig. 3 is completed. (inset) Widths  $\delta_M$  of the avoided crossings between  $|e; +\frac{3}{2}\rangle$  and  $|f; M\rangle$  versus applied electric field, at their respectively maximizing values of  $\theta_{EB}$ .  $\delta_{+1/2}$  is linear with field, while  $\delta_{-1/2}$  and  $\delta_{-3/2}$  are cubic. (b) Time-of-flight trace of trap oscillations, observed by loading the trap with a non-zero center-of-mass velocity. The solid red fit yields a trap frequency  $\nu_{trap} = 675$  Hz.

cillation frequency  $\nu_{trap}$  observed in Fig. 4(b). As both  $\delta_{-1/2}$  and  $\delta_{-3/2}$  are third-order in  $E$ , the most striking feature of the Landau-Zener model is that it explains the extremely steep rise in  $\Gamma$ :  $\Gamma \sim 1 - \exp(-\alpha E^6)$  where  $\alpha$  represents the Landau-Zener parameters.

The success of this model prompts two conclusions. The first is that magnetic trapping of the lower parity doublet in any molecule is fraught with difficulties: in OH, even just the fields from stray charge accumulating on the trap mounts is enough to cause unity loss through the  $X_{+1/2}$  channel. (We are currently implementing a new trap mount design to minimize the patch charges in our future work.) In general, if one wishes to explore polar radicals in mixed fields in any states except the doubly-stretched ones, either optical trapping or an Ioffe-Pritchard trap with a sufficiently large offset  $B$ -field as to be above all the crossings is necessary; this implies that polar radicals in their lower parity doublet are extremely challenging candidates for slowing with a magnetic coil-gun [27, 28]. More broadly, in precision measurement applications it is imperative to take a close look [29] at the exact Stark-Zeeman spectrum of the system of inter-

est, as the spectral distortions from the avoided crossings can persist over very large ranges in magnetic field.

This work was funded by DOE, the AFOSR MURI on Cold Molecules, NSF, and NIST. M. Hummon is an National Research Council postdoctoral fellow.

\* stuhl@jila.colorado.edu

† Present address: Ion Storage Group, National Institute of Standards and Technology, Boulder, CO 80305, USA

- [1] J. D. Weinstein, R. deCarvalho, T. Guillet, B. Friedrich, and J. M. Doyle, *Nature* **395**, 148 (1998).
- [2] H. L. Bethlem, G. Berden, and G. Meijer, *Phys. Rev. Lett.* **83**, 1558 (1999).
- [3] J. R. Bochinski, E. R. Hudson, H. J. Lewandowski, G. Meijer, and J. Ye, *Phys. Rev. Lett.* **91**, 243001 (2003).
- [4] S. Ospelkaus, K.-K. Ni, D. Wang, M. H. G. de Miranda, B. Neyenhuis, G. Quémener, P. S. Julienne, J. L. Bohn, D. S. Jin, and J. Ye, *Science* **327**, 853 (2010).
- [5] K.-K. Ni, S. Ospelkaus, D. Wang, G. Quémener, B. Neyenhuis, M. H. G. de Miranda, J. L. Bohn, J. Ye, and D. S. Jin, *Nature* **464**, 1324 (2010).
- [6] B. C. Sawyer, B. K. Stuhl, M. Yeo, T. V. Tscherebul, M. T. Hummon, Y. Xia, J. Klos, D. Patterson, J. M. Doyle, and J. Ye, *Phys. Chem. Chem. Phys.* **10**, 1039/C1CP21203F.
- [7] M. H. G. de Miranda, A. Chotia, B. Neyenhuis, D. Wang, G. Quémener, S. Ospelkaus, J. L. Bohn, J. Ye, and D. S. Jin, *Nat. Phys.* **7**, 502 (2011).
- [8] E. R. Hudson, H. J. Lewandowski, B. C. Sawyer, and J. Ye, *Phys. Rev. Lett.* **96**, 143004 (2006); B. L. Lev, E. R. Meyer, E. R. Hudson, B. C. Sawyer, J. L. Bohn, and J. Ye, *Phys. Rev. A* **74**, 061402 (2006).
- [9] J. J. Hudson, D. M. Kara, I. J. Smallman, B. E. Sauer, M. R. Tarbutt, and E. A. Hinds, *Nature* **473**, 493 (2011).
- [10] J. L. Bohn, *Phys. Rev. A* **63**, 052714 (2001).
- [11] C. Ticknor and J. L. Bohn, *Phys. Rev. A* **72**, 032717 (2005).
- [12] L. Santos, G. V. Shlyapnikov, P. Zoller, and M. Lewenstein, *Phys. Rev. Lett.* **85**, 1791 (2000).
- [13] G. Pupillo, A. Griessner, A. Micheli, M. Ortner, D.-W. Wang, and P. Zoller, *Phys. Rev. Lett.* **100**, 050402 (2008).
- [14] B. C. Sawyer, B. K. Stuhl, D. Wang, M. Yeo, and J. Ye, *Phys. Rev. Lett.* **101**, 203203 (2008).
- [15] A. Micheli, G. K. Brennen, and P. Zoller, *Nat. Phys.* **2**, 341 (2006).
- [16] A. O. G. Wallis, S. A. Gardiner, and J. M. Hutson, *Phys. Rev. Lett.* **103**, 083201 (2009).
- [17] E. R. Meyer and J. L. Bohn, *Phys. Rev. A* **83**, 032714 (2011).
- [18] B. C. Sawyer, B. L. Lev, E. R. Hudson, B. K. Stuhl, M. Lara, J. L. Bohn, and J. Ye, *Phys. Rev. Lett.* **98**, 253002 (2007).
- [19] P. S. Żuchowski, J. Aldegunde, and J. M. Hutson, *Phys. Rev. Lett.* **105**, 153201 (2010).
- [20] R. Guérout, M. Aymar, and O. Dulieu, *Phys. Rev. A* **82**, 042508 (2010).
- [21] M. Kajita, G. Gopakumar, M. Abe, and M. Hada, *Phys. Rev. A* **84**, 022507 (2011).
- [22] M. Lara, B. L. Lev, and J. L. Bohn, *Phys. Rev. A* **78**,

- 033433 (2008).
- [23] See supplemental material at [URL] for the complete OH Hamiltonian and its derivation, technical details on microwave / high voltage isolation, and further information on numerical simulations of ARP.
- [24] B. C. Sawyer, *Cold polar molecules for novel collision experiments at low energies*, Ph.D. thesis, University of Colorado (2010).
- [25] J. R. Rubbmark, M. M. Kash, M. G. Littman, and D. Kleppner, Phys. Rev. A **23**, 3107 (1981).
- [26] R. P. Feynman, F. L. Vernon, and R. W. Hellwarth, J. Appl. Phys. **28**, 49 (1957).
- [27] N. Vanhaecke, U. Meier, M. Andrist, B. H. Meier, and F. Merkt, Phys. Rev. A **75**, 031402 (2007).
- [28] E. Narevicius, A. Libson, C. G. Parthey, I. Chavez, J. Narevicius, U. Even, and M. G. Raizen, Phys. Rev. A **77**, 051401 (2008).
- [29] S. Bickman, P. Hamilton, Y. Jiang, and D. DeMille, Phys. Rev. A **80**, 023418 (2009).

# Supplemental Material to “Microwave state transfer and adiabatic dynamics of magnetically trapped polar molecules”

Benjamin K. Stuhl,\* Mark Yeo, Brian C. Sawyer,† Matt Hummon, and Jun Ye  
*JILA, National Institute of Standards and Technology and University of Colorado,  
 Department of Physics, 440 UCB, Boulder, Colorado 80309, USA*

## A. Derivation of the Stark-Zeeman Hamiltonian

In order to evaluate molecule-field interaction matrix elements of the form  $H_i = -\vec{\mu} \cdot \vec{\mathcal{F}}$  (where  $\vec{\mathcal{F}}$  represents either  $\vec{B}$  or  $\vec{E}$ ), it is necessary to transform between the molecule-fixed frame in which the appropriate dipole moment  $\vec{\mu}$  is defined and the laboratory frame in which  $\vec{\mathcal{F}}$  is defined. Following Lara et al. [1], we use the Wigner rotation matrix elements  $\mathcal{D}_{qk}^{1*}(\omega)$  to write

$$H_i = -\vec{\mu} \cdot \vec{\mathcal{F}} = -\sum_q (-1)^q \left( \sum_k \mathcal{D}_{qk}^{1*}(\omega) \mu_k \right) \mathcal{F}_{-q}.$$

While OH is not fully a Hund’s case (a) molecule, it is nonetheless close enough that both the electric and magnetic dipole moments may be considered to lie along the internuclear axis and so  $H_i$  simplifies to

$$H_i = -\sum_q (-1)^q \mathcal{D}_{q0}^{1*}(\omega) \mu_{k=0} \mathcal{F}_{-q}.$$

If  $\vec{B}$  and  $\vec{E}$  are not parallel, it is further necessary to rotate the laboratory fields to a combined frame. Without loss of generality, we choose  $Z$  along  $\vec{B}$  and transform  $\vec{E}$  using the reduced rotation matrix elements  $d_{qk}^{1*}(\theta_{EB})$  to write

$$H_i = -\mathcal{D}_{00}^{1*}(\omega) \mu_{k=0}^{(B)} |B| - \sum_q \mathcal{D}_{q0}^{1*}(\omega) \mu_{k=0}^{(E)} d_{-q0}^{1*}(\theta_{EB}) |E|.$$

Using Lara et al.’s results for the  $|JM\bar{\Omega}\epsilon\rangle$  parity basis yields the matrix elements

$$\begin{aligned} \langle JM\bar{\Omega}\epsilon | H_i | J'M'\bar{\Omega}'\epsilon' \rangle &= \sqrt{2J+1}\sqrt{2J'+1} \begin{pmatrix} J & 1 & J' \\ -\bar{\Omega} & 0 & \bar{\Omega}' \end{pmatrix} (-1)^{M-\bar{\Omega}} \\ &\times \left\{ \left( \frac{1 + \epsilon\epsilon' (-1)^{J+J'+2\bar{\Omega}}}{2} \right) \begin{pmatrix} J & 1 & J' \\ -M & 0 & M' \end{pmatrix} \mu_B B (\Lambda + g_e \Sigma) \right. \\ &\left. + \left( \frac{1 - \epsilon\epsilon' (-1)^{J+J'+2\bar{\Omega}}}{2} \right) \sum_q \begin{pmatrix} J & 1 & J' \\ -M & q & M' \end{pmatrix} d_{-q0}^{1*}(\theta_{EB}) \mu_e E \right\} \end{aligned}$$

where  $g_e$  is the electron Landé  $g$ -factor and  $\mu_e$  is the molecular electric dipole moment.

\*Electronic address: stuhl@jila.colorado.edu

†Present address: Ion Storage Group, National Institute of Standards and Technology, Boulder, CO 80305, USA

## B. Full OH Hamiltonian

Evaluating the matrix elements described previously for the OH  $|J = \frac{3}{2}, M, \bar{\Omega} = \frac{3}{2}, \epsilon\rangle$  ground state manifold yields the  $8 \times 8$  matrix used for combined Stark-Zeeman calculations in this paper:

$$\begin{pmatrix} -\frac{\Delta}{2} - \frac{6}{5}\mu_B B & 0 & 0 & 0 & \frac{3}{5}\mu_e E \cos \theta_{EB} & -\frac{\sqrt{3}}{5}\mu_e E \sin \theta_{EB} & 0 & 0 \\ 0 & -\frac{\Delta}{2} - \frac{2}{5}\mu_B B & 0 & 0 & -\frac{\sqrt{3}}{5}\mu_e E \sin \theta_{EB} & \frac{1}{5}\mu_e E \cos \theta_{EB} & -\frac{2}{5}\mu_e E \sin \theta_{EB} & 0 \\ 0 & 0 & -\frac{\Delta}{2} + \frac{2}{5}\mu_B B & 0 & 0 & -\frac{2}{5}\mu_e E \sin \theta_{EB} & -\frac{1}{5}\mu_e E \cos \theta_{EB} & -\frac{\sqrt{3}}{5}\mu_e E \sin \theta_{EB} \\ 0 & 0 & 0 & -\frac{\Delta}{2} + \frac{6}{5}\mu_B B & 0 & 0 & -\frac{\sqrt{3}}{5}\mu_e E \sin \theta_{EB} & -\frac{3}{5}\mu_e E \cos \theta_{EB} \\ \frac{3}{5}\mu_e E \cos \theta_{EB} & -\frac{\sqrt{3}}{5}\mu_e E \sin \theta_{EB} & 0 & 0 & \frac{\Delta}{2} - \frac{6}{5}\mu_B B & 0 & 0 & 0 \\ -\frac{\sqrt{3}}{5}\mu_e E \sin \theta_{EB} & \frac{1}{5}\mu_e E \cos \theta_{EB} & -\frac{2}{5}\mu_e E \sin \theta_{EB} & 0 & 0 & \frac{\Delta}{2} - \frac{2}{5}\mu_B B & 0 & 0 \\ 0 & -\frac{2}{5}\mu_e E \sin \theta_{EB} & -\frac{1}{5}\mu_e E \cos \theta_{EB} & -\frac{\sqrt{3}}{5}\mu_e E \sin \theta_{EB} & 0 & 0 & \frac{\Delta}{2} + \frac{2}{5}\mu_B B & 0 \\ 0 & 0 & -\frac{\sqrt{3}}{5}\mu_e E \sin \theta_{EB} & -\frac{3}{5}\mu_e E \cos \theta_{EB} & 0 & 0 & 0 & \frac{\Delta}{2} + \frac{6}{5}\mu_B B \end{pmatrix}.$$

## C. Microwave coupling circuit design

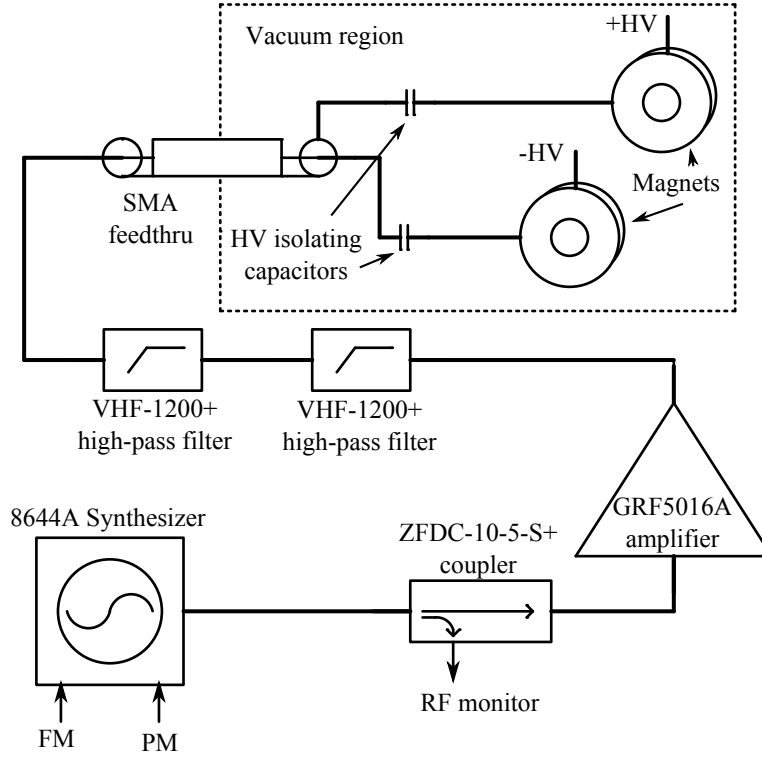


Figure S1: A schematic of the microwave system use to transfer OH between  $\Lambda$ -doublet levels.

In order to couple microwave power on to our trap magnets while protecting the microwave system from the  $\pm 14$  kV applied to the magnets during the trap loading sequence, we use a pair of custom in-vacuum capacitors to block the DC high voltage plus two more high-pass filters (Mini-Circuits VHF-1200+[2]) to block the AC transients generated by the magnet switching.

Tunable microwave power is generated by an HP 8644A synthesizer, which is programmed to form the ARP pulse by voltages supplied to its frequency and pulse modulation inputs. A Mini-Circuits ZFDC-10-5-S+ directional coupler allows monitoring of the microwave signal before it is amplified by a GTC GRF5016A power amplifier. The microwaves are then coupled through the protection filters and into the vacuum system via an SMA feedthru. Typical power levels are 30.4–35.4 dBm (1–3 W) at the feedthru. As the ARP chirp time  $\tau_{ARP}$  must be much shorter than  $\tau_{dyn}$ ,  $\tau_{ARP}$  is generally between 20 and 80  $\mu$ s.

### D. Numerical simulations of ARP

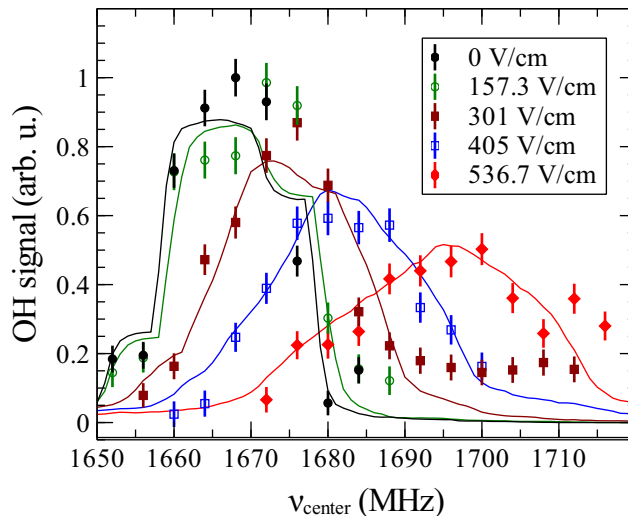


Figure S2: ARP spectra at several different bias  $E$ -fields. Points are data while solid lines are simulation results. The Stark-Zeeman broadening due to the avoided crossings is clearly visible.

As described in the main text, we have performed numerical simulations of the ARP population dynamics. The simulation code works as follows:

1. For each molecule in a Monte Carlo distribution, the Optical Bloch Equations are solved using the local magnitude of the microwave field (the microwave field is assumed to follow the DC field distribution generated by charging the magnet surfaces) and its angle against the local magnetic field. Both field distributions were calculated using a finite-element package. The final probability of the molecule transferring to the lower  $\Lambda$ -doublet state is then recorded.
2. For each molecule, the local static  $E$ -field is calculated and then combined with the local  $B$ -field to find the total Stark-Zeeman detuning. This yields a transfer probability density as a function of microwave frequency.
3. The probability density function is then integrated over the range of frequencies the ARP chirp sweeps through to get a final transfer probability.

Figure S2 shows several ARP spectra at different bias  $E$ -fields. The agreement between data (points) and simulation (solid lines) is good; in particular, the simulations capture the Stark-Zeeman broadening visible at larger fields. In a homogeneous field and the absence of avoided crossings, the application of an  $E$ -field would merely push the two  $\Lambda$ -doublet states apart without broadening the transition. The field in the trap region is not fully homogeneous, which contributes some broadening, while the curvature of the  $|e; M = +\frac{3}{2}\rangle$  state near its avoided crossings further increases the Stark-Zeeman broadening. In order to fit the simulations to the data, a background stray  $E$ -field on the order of 120 V/cm was required, consistent with the field required for the Landau-Zener model.

- 
- [1] Manuel Lara, Benjamin L. Lev, and John L. Bohn. Loss of molecules in magneto-electrostatic traps due to nonadiabatic transitions. *Phys. Rev. A*, 78(3):033433, Sep 2008.
- [2] Manufacturer and part names are listed for completeness only and do not constitute an endorsement by NIST.